Pathogenesis and Classification of Chiari Malformation Type I Based on the Mechanism of Ptosis of the Brain Stem and Cerebellum: A Morphometric Study of the Posterior Cranial Fossa and Craniovertebral Junction

Misao Nishikawa[1,2,3] Paolo A. Bolognese[2,4] Roger W. Kula[2,4] Hiromichi Ikuno[1] Kenji Ohata[3]

[1] Department of Neurosurgery, Moriguchi-Ikuno Memorial Hospital Koudoukai Health System, Osaka, Japan
[2] The Chiari Institute, North Shore University Hospital, New York, United States
[3] Osaka City University Graduate School of Medicine, Neurosurgery, Osaka, Japan
[4] Chiari Neurosurgical Center, Long Island, New York, United States

Address for correspondence Misao Nishikawa, MD, PhD, Moriguchi-Ikuno Memorial Hospital, 6-17-33 Satanakamachi, Moriguchi City, Osaka 570-0002, Japan (e-mail: misaonishikawa88@gmail.com).

J Neurol Surg B 2021;82:277–284.

Abstract

Introduction We investigated the mechanism of ptosis of the brain stem and cerebellum (hindbrain) in Chiari malformation type I (CM-I) and classified CM-I according to pathogenesis, based on a morphometric study of the posterior cranial fossa (PCF) and craniovertebral junction (CVJ). We discuss the appropriate surgical treatment for hindbrain ptosis.

Materials and Methods We examined 500 patients with CM-I and 100 healthy control individuals. We calculated the volume of the PCF (VPCF) and measured the axial length of the enchondral parts of the occipital bone and hindbrain. As statistical analyses, for the multiple analyses, heavy palindromic tests were used. Using three independent objective parameters, we tried to classify CM-I.

Results Three independent subtypes were confirmed (CM-I types A, B, and C). CM-I type A (167 cases): normal VPCF, normal volume of the area surrounding the foramen magnum (VSFM), and normal occipital bone size; CM-I type B (178 cases): normal VPCF, small VSFM, and small occipital bone size; and CM-I type C (155 cases): small VPCF, small VSFM, and small occipital bone size.

Conclusions Morphometric analyses of PCF and CVJ were very useful for the investigation of the mechanism of hindbrain ptosis and classifying CM-I according to pathogenesis. CM-I type A included mechanisms other than hindbrain ptosis, for example, CVJ instability, tethered cord, and increased intracranial pressure. CM-I types B and C demonstrated underdevelopment of the occipital bone. For CM-I types B and C, posterior decompression should be performed. For CM-I type A, appropriate surgical management should be selected.

Keywords
- Chiari malformation
- morphometric study
- posterior cranial fossa
- craniovertebral junction
- surgical management

received
October 7, 2018
accepted after revision
March 31, 2019
published online
September 30, 2019

DOI https://doi.org/10.1055/s-0039-1691832.
ISSN 2193-6331.

Introduction

Previously, we reported that patients with a Chiari malformation (CM) have an underdeveloped occipital bone, so that the posterior cranial fossa becomes shallow.[1–3] This shallowness results in the brain stem and cerebellum sagging into the spinal canal, so a CM is caused by insufficiency of the para-axial mesoderm, from which the occipital bone originates.[1–3] Several reports have provided support for our hypothesis and the pathogenic mechanism,[4–8] while developmental biology studies have provided further support by demonstrating that genetic abnormalities influence segmentation of the paraxial mesoderm.[9,10] Other mechanisms causing ptosis of the brain stem and cerebellum, that is, instability of the craniovertebral junction, traction by tethering, and pressure coning, have also been described.[11–15] Misunderstandings of the mechanism of ptosis of the brain stem and cerebellum in CM have resulted in confusion when choosing a surgical approach, and the use of inappropriate treatment has resulted in the recurrence of neurological symptoms. It is entirely necessary to define and classify CMs; however, a diagnostic strategy clearly demonstrating the mechanism of ptosis of the brain stem and cerebellum has not been developed.

Since 2006, we have performed morphometric studies of the posterior cranial fossa using magnetic resonance imaging (MRI) and computed tomography (CT) reconstructed images, the approach for which was designed and established by the authors, and have conducted multiple analyses on cases with a CM.[1–3] In the present study, we examined the mechanism underlying ptosis of the brain stem and cerebellum using morphometric analysis to redefine and classify CM-I. We also discuss surgical approaches to treat the mechanism of ptosis of the brain stem and cerebellum.

Materials

We recruited 100 healthy control volunteers with no neurological symptoms or abnormalities in the neural axis (16–69 years old, mean: 38.7 years, 40 males, 60 females). For the cases, 500 subjects with CM-I (cerebellar tonsil herniation $\geq$ 5 mm from the McRae line, i.e., between the basion and opisthion) (16–69 years old, mean: 37.7 years, 272 males, 328 females), 30 subjects with CM-II associated with spina bifida (meningocele) (16–31 years old, mean: 21.5 years, 12 males, 18 females), and 50 subjects with an absence of CM-I (defined as cerebellar tonsil herniation $<$ 5 mm from the McRae line, but having brain stem symptoms and/or myelopathy due to associated syringomyelia) (17–55 years old, mean: 35.4 years, 18 males, 32 females) were examined. The distribution and mean of age and sex were not significantly different between the normal controls and CM-I group. CM-I was associated with syringomyelia in 221 cases, hereditary disorders in connective tissue in 187 cases, and basilar invagination (23 cases) and other bony anomalies in the craniovertebral junction in 57 cases. These patients were diagnosed and treated from April 2006 to March 2017.

Methods: Volumetric and Morphometric Analyses

Morphometric Analyses

By MRI, analysis of two-dimensional (2D)- and/or 3D-CT reconstructed images with Osirix software (free access) was used to calculate the volume of the posterior cranial fossa (VPCF), volume of the area surrounding the foramen magnum (VSFM), which was defined as the sum total of the areas at two levels: (1) the inferior outlet between the basion and opisthion; and (2) the superior outlet at the top of the jugular tubercles, and volume of the brain (midbrain, pons, medulla oblongata, and cerebellum excepting herniated brain) in the posterior cranial fossa (VPCB) (►**Figs. 1** and **2**).[1–3] VPCF was divided into the volume above Twining's line (the line between the tubercle sellar and internal occipital protuberance) (VPCF-ATL) and below Twining's line (VPCF-BTL). The axial length of the basiocciput, exocciput, supraocciput as enchondral as enchondral parts of the occipital bone (occipital bone size), and axial length of the brain stem (BSL), cerebellum (excluding herniated tonsils), and the position of the brain stem and fourth ventricle were also measured (►**Figs. 1** and **2**).[1–3] By multiple analyses of the results, CM-I was classified.

The first author (MN: neurosurgeon), third author (PB: neurosurgeon), fourth author (RK: neurologist), and last author (HI: neuroradiologist) performed the measurements. MN and RK performed the statistical analyses. The first author (MN) wrote the manuscript. The last author (KO) conducted and supported this study.

Instability of the Craniovertebral Junction and Tethered Cord Syndrome

Diagnosis of instability at the craniovertebral junction was confirmed by a morphometric study and craniocervical traction test, using morphometric analyses described by the authors and Goel et al.[11–14] The first author (MN: neurosurgeon), second author (TM: neurosurgeon), and third author (PA: neurosurgeon) performed the craniocervical traction test and measurements. For the craniocervical traction test, a tong was attached to the skull under intravenous anesthesia in the supine position and morphometric measurements were performed. Then, the patient was placed in an upright position and craniocervical instability was revealed as neurological symptoms (checked by the fourth author, RK: neurologist), and when morphometric measurements were taken, displacement at the occipito-atlanto-axial joints ($>$1 standard deviation [SD]) was observed. Craniocervical traction of 10 to 15 kg was then applied and the neurological symptoms resolved (checked by the fourth author. RK: neurologist) and a reduction in the craniocervical junction was observed.

Diagnosis of tethered cord syndrome was determined by neurological symptoms (e.g., motor weakness at both lower extremities, sensory loss, neurogenic bladder, pes equinus, and the conus medullaris lower than the L2 vertebral body and/or the diameter of the filum terminale $\geq$ 2 mm).[15] The fourth author (RK: neurologist) diagnosed tethered cord syndrome.

Statistical Analysis

IBM SPSS statistics (IBM, Inc., Chicago, Illinois, United States) was used for statistical analyses. For the comparison of means between two groups, the Mann–Whitney U test was used. For the comparison of more than two groups, the Kruskal–Wallis test was used. A p-value < 0.01 was used to determine significance. For the multiple analyses, heavy palindromic tests were used.

Results

The volume of the brain stem and cerebellum and morphometric analyses (axial length of the brain stem and cerebellum) indicated there was no significant difference between the cases and healthy controls. Of the measured items, the following variables were significantly different in the cases compared with the healthy controls: VPCF, the ratio of VPCB to VPCF (VPCB/VPCF), occipital bone size (axial length of the basiocciput, exocciput, and supraocciput), and VSFM. By using palindromic tests in multifactorial analyses, three parameters (VPCF, VSFM, and occipital bone size) were used to classify the CM-I group into three independent groups: CM-I types A, B, and C. A pathological condition was defined when VPCF, VSFM, and occipital bone size were <2 SD.

In CM-I type A (167 cases), there was no significant difference compared with the normal controls in VPCF, VSFM, and occipital bone size (►**Table 1** and ►**Fig. 3**). The volume of the brain stem and cerebellum was not significantly different compared with the normal controls.

In CM-I type B (178 cases), there was no significant difference compared with the normal controls in VPCF, but VSFM and occipital bone size were significantly smaller. In this group, VPCF-ATL and VPCF-BTL were significantly smaller than in the other groups (►**Table 1** and ►**Fig. 3**).

In CM-I type C (155 cases), VPCF, VSFM, and occipital bone size were significantly smaller than in the normal controls. In this group, VPCF-ATL and VPCF-BTL were significantly smaller than in the other groups (►**Table 1** and ►**Fig. 3**). Moreover, BSL was significantly longer than in the other groups, suggesting elongation of the brain stem in CM-I type C.

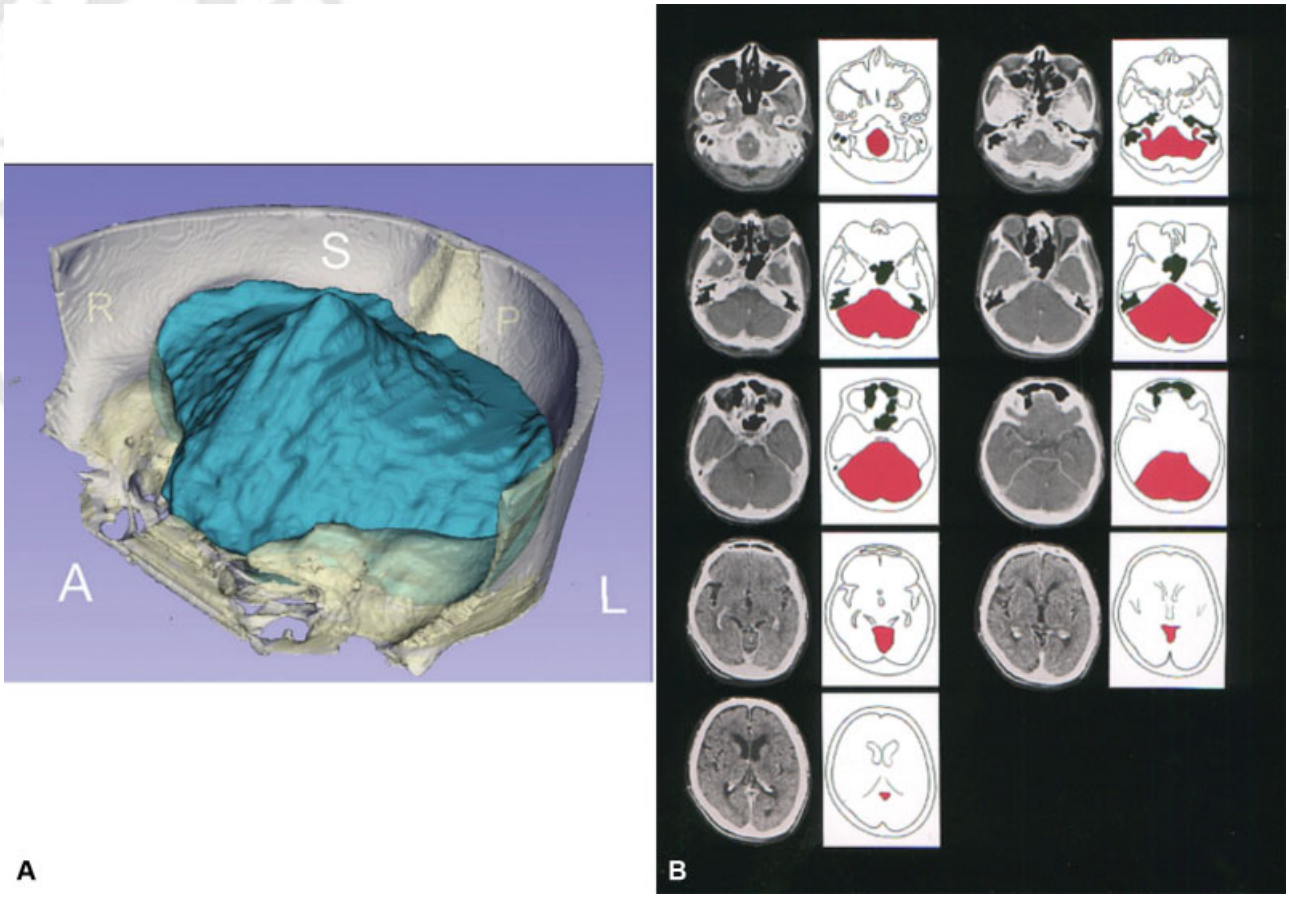

Fig. 1 Calculation of the volume of the posterior cranial fossa (PCF). (**A**) Three-dimensional (3D) reconstructed image of the PCF using Osirix software. (**B**) Two-dimensional (2D)-computed tomography (CT) images of the PCF. The PCF was defined as the almost circular space bounded by the tentorium cerebelli, occipital bone, clivus, petrous bone, and petrous ridges. The ridges of the petrous bones form the anterolateral border of the cavity, and their connection to the posterior clinoids (posterior petroclinoid ligament) forms the anterior border. The caudal end of the PCF was defined as the foramen magnum including McRae's line. McRae's line was defined as the line between the basion and opisthion. The volume of brain in the posterior cranial fossa (VPCB) was calculated as the neural content of the PCF including the cerebellum, mesencephalon, pons, and medulla (blue areas in the left panel and red areas in the right panel). Volumetric calculations were performed using 3D radiographic analysis software (Osirix). The volume of the PCF (VPCF) was calculated using reconstructed 2D-CT images, and VPCB was calculated on magnetic resonance axial and sagittal images, excluding the fourth ventricle and herniated cerebellar tonsils and medulla. VPCF was divided into the volume above Twining's line (the line between the tubercle sellar and internal occipital protuberance) and below Twining's line.

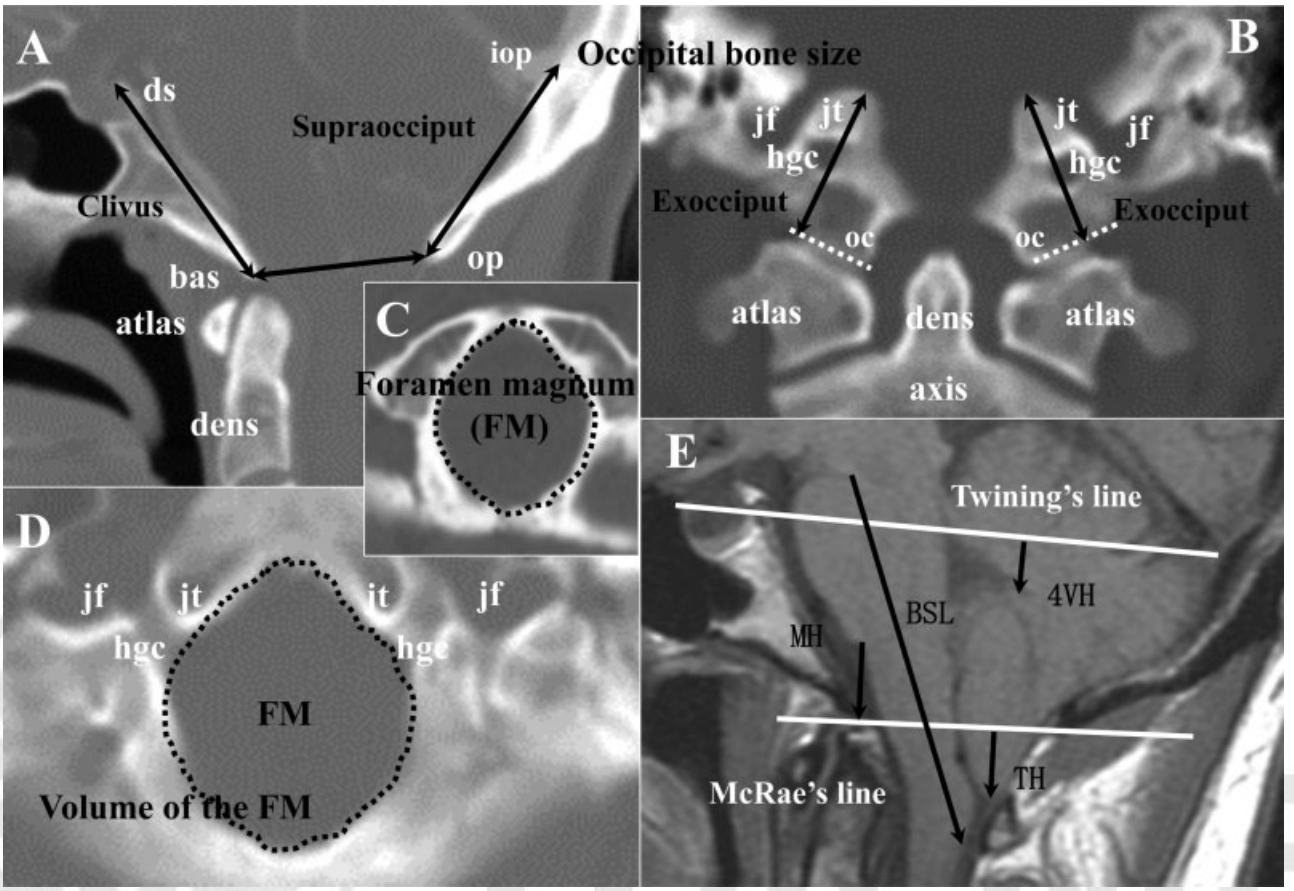

Fig. 2 Morphometric analysis of the posterior cranial fossa. (**A**) Two-dimensional (2D) reconstructed computed tomography (CT) sagittal image demonstrating morphometric measurements of the basiocciput, supraoccput, and anterior–posterior diameter of the foramen magnum (FM). (**B**) 2D reconstructed coronal image demonstrating morphometric measurements of the exoccput. (**C**) 2D reconstructed CT image demonstrating the area of the inferior outlet of the FM at the level of the basion and opisthion. (**D**) 2D reconstructed CT image demonstrating the area of the superior outlet of the FM at the level of the jugular tubercle. (**E**) Magnetic resonance midline sagittal image demonstrating morphometric measurements of the brain stem and cerebellum, medullary height (MH), and the position of the fourth ventricle. ds, top of the dorsum sellae; hgc, hypoglossal canal; iop, internal occipital protuberance; jf, jugular foramen; jt, jugular tubercle; oc, occipital condyle; ts, tuberculum sellae. Twining's line: the line between the tuberculum sellae and internal occipital protuberance. Using reconstructed 2D-CT and magnetic resonance imaging scans of the head, the size of the occipital bone was determined by measuring its enchondral parts (exoccput, basiocciput, and supraoccput), which enclose the posterior cranial fossa (►**Fig. 1**). Measurements included the axial length of the clivus (basiocciput and basisphenoid) from the top of the dorsum sella to the basion; the axial length of the supraoccput from the center of the internal occipital protuberance to the opisthion; and the axial length of the occipital condyle (exoccput) from the top of the jugular tubercle to the bottom of the occipital condyle and the supraoccput (distance between the opisthion and the center of the internal occipital protuberance): these three measurements were unified as occipital bone size. The volume of the surrounding area of the foramen magnum was defined as the sum total of areas on two levels: (1) the inferior outlet between the basion and opisthion; and (2) the superior outlet at the level of the top of the jugular tubercles. The axial length of the brain stem was measured between the midbrain-pons junction and medullocervical junction. MH was defined as the vertical distance between the pontomedullary junction and foramen magnum. The position of the fourth ventricle was defined as the vertical distance between the top of the fourth ventricle and Twining's line. TH means the length of herniation of the cerebellar tonsils. Radiographic analysis software (Osirix: free access) was used for measurements and calculations.

In CM-II (30 cases), VPCF and occipital bone size were significantly smaller than in the normal controls, while BSL was longer, similar to the pattern observed in CM-I type C. However, VSFM was significantly larger than in the normal controls (►**Table 1** and ►**Fig. 3**). In addition, VSFM was significantly larger in CM-I type B than in CM-I type A.

In CM-absence (30 cases), there was no significant difference in VPCF compared with the normal controls, but occipital bone size and VSFM were significantly smaller (►**Table 1**).

In CM-I type B, CM-I type C, and CM-II, the VPCB/VPCF ratio was significantly larger than in the other groups, indicating the narrowness of the posterior cranial fossa. In CM-I type A, CM-I type C, and CM-II, BSL was significantly longer and the pontomedullary junction and the position of the top of the fourth ventricle was significantly lower than in the other groups. There were 5 CM-I type A cases, 7 CM-I type B cases, and 10 CM-I type C cases with basilar invagination. The 17 cases with another lesion had a mass lesion in the posterior cranial fossa, an arachnoid cyst, and secondary pathogenesis.

Discussion

In the present study, we demonstrated that CM-I could be divided into three subgroups: CM-I types A, B, and C. VPCF

Table 1 Results of volumetric analyses and morphometric measurements: Chiari malformation Type I (CM-I)

	Normal controls	CM-I type A	CM-I type B	CM-I type C	CM-II	CM-absence
Total no. of cases	100	167	178	155	30	50
Male and female	35 and 65	80 and 87	83 and 95	74 and 81	12 and 18	12 and 32
Age	16–69 years old	16–69 years old	17–64 years old	16–59 years old	16–31 years old	17–55 years old
Mean age (y)	38.7 ± 10.2	39.6 ± 10.1	37.8 ± 10.8	33.4 ± 10.3	18.7 ± 10.2	42.4 ± 10.4
Occipital bone size						
Clivus: axial length (mm)	47.5 ± 3.55	47.4 ± 3.54	40.5 ± 3.50[a]	45.6 ± 3.24[a]	48.6 ± 3.24[a]	47.4 ± 3.36
Supraoccipital axial length (mm)	46.8 ± 3.64	47.8 ± 3.62	86.8 ± 3.64[a]	46.3 ± 3.43[a]	46.3 ± 3.43[a]	47.8 ± 3.77
Condyle axial height at the right (mm)	24.0 ± 3.24	24.0 ± 3.24	20.0 ± 3.42[a]	23.5 ± 3.22[a]	23.5 ± 3.22[a]	24.0 ± 3.24
Condyle axial height at the left (mm)	23.9 ± 3.32	23.9 ± 3.32	20.9 ± 3.25[a]	23.9 ± 3.31[a]	23.9 ± 3.31[a]	23.9 ± 3.32
Volumetric analysis						
VPCF (mL)	189.4 ± 8.77	189.8 ± 8.75	189.4 ± 8.77	182.4 ± 8.77[a]	180.4 ± 8.77	189.5 ± 8.54
VPCF-ATL (mL)	44.2 ± 5.10	44.2 ± 5.12	44.2 ± 5.10[b]	38.5 ± 5.14[a]	38.5 ± 5.14	44.8 ± 5.32
VPCF-BTL (mL)	147.6 ± 4.38	145.6 ± 4.45	124.0 ± 5.44	144.0 ± 7.31	142.0 ± 7.31	145.0 ± 4.47
VSFM (mL)	25.3 ± 3.22	25.4 ± 3.24	20.3 ± 3.43[a]	18.8 ± 3.34[a]	30.8 ± 3.34[b]	21.2 ± 3.53[a]
PCB (mL)	150.1 ± 3.13	151.2 ± 3.14	150.1 ± 3.46	152.1 ± 3.23	152.1 ± 3.23	150.8 ± 3.43
Neural structures						
Brain stem length (mm)	51.2 ± 2.34	51.2 ± 2.32	51.3 ± 2.44	61.3 ± 2.23[b]	65.2 ± 2.23[b]	51.0 ± 2.65
Medullary height (mm)	18.4 ± 4.25	10.4 ± 4.27[a]	18.4 ± 4.27	14.4 ± 4.63[a]	11.4 ± 4.63[a]	18.8 ± 4.43
Fourth ventricle height (mm)	4.18 ± 3.12	1.17 ± 3.14[b]	4.15 ± 3.15	8.18 ± 3.12[b]	7.10 ± 3.12[b]	4.20 ± 3.52

Abbreviations: CM-absence, cases with neurological brain stem symptoms, but tonsillar herniation less than 5 mm; CM-II, Chiari malformation type II; VPCF, volume of the posterior cranial fossa; VPCF-ATL, volume pf the posterior cranial fossa above Twining's line; VPCF-BTL, volume of the posterior cranial fossa below Twining's line; VSFM, volume of the area surrounding the foramen magnum; VPCB, volume of the brain in the posterior cranial fossa.
Results are expressed as mean with ± one standard deviation.
[a]Significantly smaller or shorter than those of normal controls ($p < 0.01$).
[b]Significantly longer or larger than those of normal controls ($p < 0.01$).

was normal in CM-I types A and B, but was small in CM-I type C. VSFM and occipital bone size were small in CM-I types B and C, while in CM-I types B and C, the VPCB/VPCF ratio was high, indicating the narrowness of the posterior cranial fossa, so that the brain stem and cerebellum herniated into the spinal canal. In CM-I type B, the increase in VPCF-ATL by the steepness of the cerebellar tentorium compensated for the reduction of VPCF-BTL, and so the volume of the entire posterior cranial fossa was normal.

Mechanisms: Pathogenesis of Ptosis of the Brain Stem and Cerebellum in CM-I Types B and C

Ptosis of the brain stem and cerebellum was caused by a small VSFM and underdevelopment of the occipital bone (►**Table 2** and ►**Fig. 3**). From the embryological point of view, the occipital bone is formed from the enchondral bone, which originates from occipital somites. Therefore, the pathogenesis of CM-I types B and C was insufficiency of the para-axial mesoderm, as the source of the occipital bone. Fischl et al proved that the occipital enchondral bone developed from occipital somites originating from the paraxial mesoderm.[10] Speer et al proved the existence of a mutation in an unidentified gene that influenced segmentation of the mesoderm and neural tube.[9] Milhorat et al reported that there were some families with CM-I with an underlying genetic basis that was inherited in an autosomal dominant manner.[2]

In subjects with CM-I type C, the brain stem was elongated, and both the brain stem and cerebellum were displaced downward. These characteristics are similar to those observed in CM-II, except for VSFM, which was larger in CM-II. We consider that traction and/or squeezing could have caused ptosis of the brain stem and cerebellum in this setting.[16]

Mechanisms: Pathogenesis of Ptosis of the Brain Stem and Cerebellum in Craniosynostosis

Cinalli et al reported that CM-I developed in the first months of life, because of an imbalance between hindbrain growth and an abnormally small posterior fossa, a consequence of the premature fusion of the lambdoid and cranial base sutures.[17] Leikola et al reported that a statistically significant reduction in the anteroposterior diameter of the foramen magnum was found in patients with concomitant CM-I.[18]

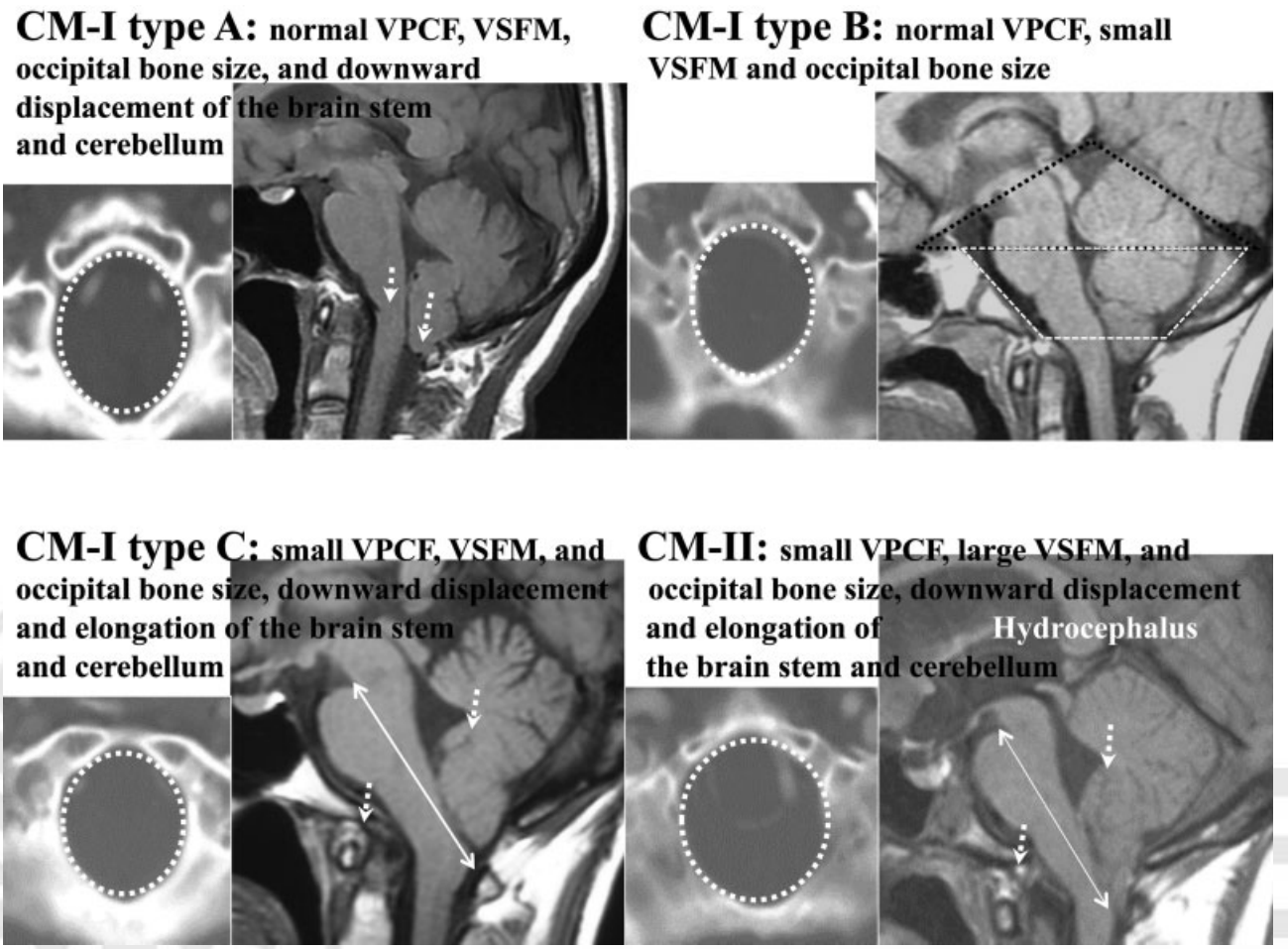

Fig. 3 Illustrative cases of Chiari malformations Chiari malformation type I (CM-I) types A upper left two images. Left: 2-dimensional (D)-computed tomography (CT) reconstructed axial image at the level of the foramen magnum; right: magnetic resonance (MR) sagittal midline image of a representative case of CM-I type A. CM-I type B: upper right two images. Left: 2D-CT reconstructed axial image at the level of the foramen magnum; right: MR midline sagittal image of a representative case of CM-I type B. CM-I type A: normal volume of the posterior cranial fossa (VPCF), normal volume of the area surrounding the foramen magnum (VSFM), and normal occipital bone size; however, downward displacement of the brain stem and 4th ventricle was observed. CM-I type B: although occipital bone size and VSFM were small, VPCF is normal because it is compensated for by the enlargement of VPCF above Twining's line owing to the steepness of the cerebellar tentorium. CM-I type C: lower left two images. Left: 2D-CT reconstructed axial image at the level of the foramen magnum; right MR sagittal midline image of a representative case of CM-I type C. Chiari malformation type II (CM-II): lower right two images. Left: 2D-CT reconstructed axial image at the level of the foramen magnum; right: MR sagittal midline image of a representative case of CM-II. CM-I type C: small VPCF, small VSFM, small occipital bone size, and downward displacement of the brain stem and 4th ventricle, as observed in CM-II. CM-II: small VPCF, large VSFM, small occipital bone size, and downward displacement of the brain stem and 4th ventricle, but large VSFM. Trapezoid black dotted area: are above Twining's line, trapezoid white dotted area: are below Twining's line, circular white dotted area: foramen magnum, arrows: axial length of the brain stem (BSL), dotted arrows: medullary height (MH) and the position of fourth ventricle.

These studies suggested that CM-I and craniosynostosis have a common cause and a genetic basis. CM-I could be understood as regional craniosynostosis limited to enchondral bone sutures surrounding the foramen magnum (basiocciput, exocciput, and supraocciput). Whitton et al used molecular biology methods to demonstrate that bone morphometric proteins and inhibitors played a significant role in the regulation of suture fusion as well in the maintenance of the patency of normal sutures.[19]

Mechanisms: Pathogenesis of Ptosis of the Brain Stem and Cerebellum in CM-I Type A

In subjects with CM-I type A, who have normal VPCF, normal VSFM, and normal occipital bone size, there was no significant difference in the VPCB/VPCF ratio compared with the normal control group (►**Table 3** and ►**Fig. 3**). Therefore, the mechanism underlying ptosis of the brain stem and cerebellum was not the narrowness of the posterior cranial fossa. Taylor et al identified two distinct population of CM based on the presence or absence of posterior cranial fossa "crowdedness" on MRI.[20] The absence of posterior fossa crowdedness suggested that it could not explain the pathogenesis of CM-I in many patients.

Milhorat et al reported the phenomenon of functional cranial settling, in which the cranium (occipital bone) falls into the craniovertebral junction.[11] This functional cranial settling could be the cause of ptosis of the brain stem and cerebellum. Goel et al also described that atlantoaxial instability could cause ptosis of the brain stem and cerebellum.[12–14] They reported evidence showing that atlantoaxial fixation resolved the instability and ptosis of the brain stem and cerebellum.[12–14]

Table 2 Pathogenesis and classification of Chiari malformation type I (CM-I) and surgical indication. Subtypes of CM-I classified, based on morphometric analyses, and surgical indication

Subtype	CM-I type A	CM-I type B	CM-I type C	CM-absence
	167 cases	178 cases	155 cases	50 cases
VPCF	Normal	Normal	Small	Normal
VSFM	Normal	Small	Small	Small
VPCB/VPCF	Normal	Large	Large	Normal
Occipital bone size	Normal	Small	Small	Normal
Pathogenesis	Others	Underdevelopment of occipital bone		
		Abnormalities of segmentation and development of		
		para-axial mesoderm		
Surgery	Others and FMD	FMD	ESCP	FMD

Abbreviations: CM-absence, cases which have neurological brain stem symptoms but tonsillar herniation less than 5 mm; CM-I, Chiari malformation type I; ESCP, expansive suboccipital cranioplasty; FMD, foramen magnum decompression; PCFV, volume of the posterior cranial fossa; VSFM, volume of the area surrounding the foramen magnum; VPCB, volume of the brain in the posterior cranial fossa.

Table 3 Other mechanisms of ptosis of the brain stem and cerebellum, and surgical indications

Subtype	CVI	Traction (Tethering)	Others
	50 cases	20 cases	17 cases
VPCF	Normal	Normal	Normal
VSFM	Normal	Normal	Normal
VPCB/VPCF	Normal	Normal	
Brain stem and Cerebellum	Normal	Elongation and/or downward displacement	
Pathogenesis	FCS	Tethered cord syndrome	Pressure dissociation
Surgery	CCF	Untethering and/or SFT	VPS and/or others

Abbreviations: CVI, craniovertebral instability; VPCF, volume of the posterior crania fossa; VSFM, volume of the area surrounding the foramen magnum; VPCB, volume of the brain in the posterior cranial fossa; FCS, functional cranial settling; CCF, cranio-cervical fixation; SFT, sectioning of the filum terminale; VPS, ventriculo peritoneal shunt.

In addition, Milhorat et al indicated that tethering could cause ptosis of the brain stem and cerebellum by a traction effect. Traction at the tethering regions of the spinal cord and brain stem with the cerebellum could cause their downward displacement into the spinal canal. In CM-I type A, various mechanisms could cause ptosis of the brain stem and cerebellum.

Mechanisms: Pathogenesis of Ptosis of the Brain Stem and Cerebellum in CM-Absence

Occipital bone size and VSFM were small in subjects with CM-absence, so we considered that the mechanism of ptosis of the brain stem and cerebellum was also underdevelopment of the occipital bone and shallowness of the surrounding area of the foramen magnum, which was a very focal condition (►**Table 2**). In this type, the foramen magnum and major cistern demonstrated tightness and compression of the brain stem and cerebellar tonsils and vermis. Tubbs et al reported a similar condition in subjects with CM-0.[21] Subjects with CM-0 have tightness of the foramen magnum, but tonsillar herniation is mild and less than 5 mm, although they have neurological symptoms by compression of the brain stem and/or upper cervical cord.

Mechanisms: Pathogenesis of Ptosis of the Brain Stem and Cerebellum in CM-II

McLone and Dias reported that CM-II in children with myelomeningocele could be caused by the lack of distention of the embryonic ventricular system (►**Fig. 3**).[22] Defective occlusion and an open neural tube preclude the accumulation of fluid and pressure within the cranial vesicles. This distention is critical to normal brain and skull development. This causes overcrowding of the posterior cranial fossa and downward displacement of the hindbrain. In subjects with CM-II, the foramen magnum was large, suggesting that hindbrain displacement occurred before fusion of the enchondral bone.[23]

The brain stem and cerebellum could be squeezed through the foramen magnum into the spinal canal, according to the development of the hindbrain after birth and in the first year of life, and traction by tethering of a myelomeningocele could have caused ptosis of the brain stem and cerebellum in this setting.

Surgical Management

In the management of CM, appropriate surgical methods that can treat ptosis of the brain stem and cerebellum should be chosen (►**Tables 2** and **3**). On the basis of this idea, we selected foramen magnum decompression (FMD) for CM-I type B and CM-absence, because VSFM and occipital bone size were small. FMD consists of craniectomy to decompress the surrounding area (2–3 cm^2).[24]

Expansive suboccipital cranioplasty (ESCP), which Sakamoto and Nishikawa reported, can also be used for extensive decompression (along the transverse sinus and sigmoid sinus) and osteoplasty.[25] We chose ESCP for CM-I type C, because FMD was not considered appropriate under the setting of a small VSFM, small VPCF, and small occipital bone size.

In CM-I type A, other surgical methods that can treat ptosis of the brain stem and cerebellum must be chosen. Craniocervical fixation should be selected for cases with craniovertebral instability causing functional cranial settling.[11–14] Untethering and/or sectioning of the filum terminale should be chosen for cases with a lesion of traction and/or tethering, for example, tethered cord syndrome and thick filum terminale.[15]

Conclusion

Morphometric analyses of the posterior cranial fossa and craniocervical junction are required to investigate the mechanism of ptosis of the brain stem and cerebellum and to classify CM-I according to its pathogenesis.

CM-I can be divided into three groups (CM-I types A, B, and C) based on the VPCF, foramen magnum, and occipital bone size. The pathogenesis of CM-I types B and C and CM-absence via ptosis of the brain stem and cerebellum was considered to be underdevelopment of the occipital bone and crowdedness of the posterior cranial fossa due to paraaxial mesodermal insufficiency. The pathogenesis of CM-I type A was thought to be caused by an unspecified mechanism. Cranial settling due to craniocervical instability and traction due to tethering were considered likely causes.

Surgical intervention should be decided according to the management of the mechanism of ptosis of the brain stem and cerebellum. As surgery for CM-I type A, craniocervical fixation for cases with functional cranial settling is recommended. For tethered cord syndrome, untethering and/or sectioning of the filum terminale are suitable. For CM-I type B, FMD to enlarge VSFM is appropriate. For CM-I type C, expansive suboccipital cranioplasty is better than FMD to increase VPCF.

Conflict of Interest

The authors have no conflicts of interest to disclose.

This study has been approved by Institutional Review Board of Koudoukai Health System, Osaka City University Graduate School of Medicine, Osaka Japan, and North Shore University Hospital-LIJ, New York, USA.

Acknowledgement

The authors deeply thank Emeritus Professor of North Shore University Hospital—LIJ, Thomas H. Milhorat, M.D. for leading and supporting this study.

References

1 Nishikawa M, Sakamoto H, Hakuba A, Nakanishi N, Inoue Y. Pathogenesis of Chiari malformation: a morphometric study of the posterior cranial fossa. J Neurosurg 1997;86(01):40–47
2 Milhorat TH, Chou MW, Trinidad EM, et al. Chiari I malformation redefined: clinical and radiographic findings for 364 symptomatic patients. Neurosurgery 1999;44(05):1005–1017
3 Milhorat TH, Nishikawa M, Kula RW, Dlugacz YD. Mechanisms of cerebellar tonsil herniation in patients with Chiari malformations as guide to clinical management. Acta Neurochir (Wien) 2010;152 (07):1117–1127
4 Stovner LJ, Bergan U, Nilsen G, Sjaastad O. Posterior cranial fossa dimensions in the Chiari I malformation: relation to pathogenesis and clinical presentation. Neuroradiology 1993;35(02):113–118
5 Badie B, Mendoza D, Batzdorf U. Posterior fossa volume and response to suboccipital decompression in patients with Chiari I malformation. Neurosurgery 1995;37(02):214–218
6 Noudel R, Gomis P, Sotorares G, et al. Posterior fossa volumetric increase after surgery for Chiari malformation type I: a quantitative study of the posterior cranial fossa. J Neurosurg 2011; 115:647–658
7 Karagöz F, Izgi N, Kapíjcíjoğlu Sencer S. Morphometric measurements of the cranium in patients with Chiari type I malformation and comparison with the normal population. Acta Neurochir (Wien) 2002;144(02):165–171, discussion 171
8 Alperin N, Loftus JR, Oliu CJ, et al. Magnetic resonance imaging measures of posterior cranial fossa morphology and cerebrospinal fluid physiology in Chiari malformation type I. Neurosurgery 2014;75(05):515–522, discussion 522
9 Speer MC, George TM, Enterline DS, Franklin A, Wolpert CM, Milhorat TH. A genetic hypothesis for Chiari I malformation with or without syringomyelia. Neurosurg Focus 2000;8(03):E12
10 Fischl B, Salat DH, Busa E, et al. Whole brain segmentation: automated labeling of neuroanatomical structures in the human brain. Neuron 2002;33(03):341–355
11 Milhorat TH, Bolognese PA, Nishikawa M, McDonnell NB, Francomano CA. Syndrome of occipitoatlantoaxial hypermobility, cranial settling, and Chiari malformation type I in patients with hereditary disorders of connective tissue. J Neurosurg Spine 2007;7(06):601–609
12 Goel A, Jain S, Shah A. Radiological evaluation of 510 cases of basilar invagination with evidence of atlantoaxial instability (Group a basilar invagination). World Neurosurg 2018;110:533–543
13 Goel A, Gore S, Shah A, Dharurkar P, Vutha R, Patil A. Atlantoaxial fixation for Chiari 1 formation in pediatric age group patients: report of treatment in 33 patients. World Neurosurg 2018;111:e668–e677
14 Goel A, Kaswa A, Shah A. Atlantoaxial fixation for treatment of Chiari formation and syringomyelia with no craniovertebral bone anomaly: report an experience with 57 cases. Acta Neurochir Suppl (Wien) 2019;125:101–110
15 Milhorat TH, Bolognese PA, Nishikawa M, et al. Association of Chiari malformation type I and tethered cord syndrome: preliminary results of sectioning filum terminale. Surg Neurol 2009; 72(01):20–35
16 Geddes DM, Cargill RS, LaPlaca MC. Mechanical stretch in neurons results in a strain rate and magnitude-dependent increasing in plasma membrane permeability. J Neurotrauma Rev 2003;29:251–264
17 Cinalli G, Spennato P, Sainte-Rose C, et al. Chiari malformation in craniosynostosis. Childs Nerv Syst 2005;21(10):889–901
18 Leikola J, Haapamäki V, Karppinen A, et al. Morphometric comparison of foramen magnum in non-syndromic craniosynostosis patients with or without Chiari I malformation. Acta Neurochir (Wien) 2012;154(10):1809–1813
19 Whitton A, Hyzy SL, Britt C, Williams JK, Boyan BD, Olivares-Navarrete R. Differential spatial regulation of BMP molecules is associated with single-suture craniosynostosis. J Neurosurg Pediatr 2016;18(01):83–91
20 Taylor DG, Mastorakos P, Jane JA Jr, Oldfield EH. Two distinct populations of Chiari I malformation based on presence or absence of posterior fossa crowdedness on magnetic resonance imaging. J Neurosurg 2017;126(06):1934–1940
21 Tubbs RS, Elton S, Grabb P, Dockery SE, Bartolucci AA, Oakes WJ. Analysis of the posterior fossa in children with the Chiari 0 malformation. Neurosurgery 2001;48(05):1050–1054, discussion 1054–1055
22 McLone DG, Dias MS. The Chiari II malformation: cause and impact. Childs Nerv Syst 2003;19(7-8):540–550
23 Hatta T. Development of neural tube. Nervous System in Children 2016;41:295–302
24 Oaks J. Chiari malformation and syringomyelia. In Reagachary SS, Williams RH, eds. Principles of Neurosurgery. London: Mosby-Wolf; 19949.1.18
25 Sakamoto H, Nishikawa M, Hakuba A, et al. Expansive suboccipital cranioplasty for the treatment of syringomyelia associated with Chiari malformation. Acta Neurochir (Wien) 1999;141(09):949–960, discussion 960–961

